NJC

PAPER

View Article Online
View Journal | View Issue

Cite this: *New J. Chem.*, 2017, **41**, 2409

Synthesis, structural studies and stability of model cysteine containing DNA–protein cross-links†

Kinga Salus, Marcin Hoffmann, Tomasz Siodła, Bożena Wyrzykiewicz and Donata Pluskota-Karwatka*

DNA–protein cross-links (DPCs) are bulky, helix-distorting lesions that are formed upon irreversible bonding of proteins to chromosomal DNA in the presence of cross-linking agents. Among a broad range of such agents are α,β-unsaturated carbonyl compounds, which act essentially as bifunctional alkylating agents and form adducts with DNA bases. These adducts can further undergo interactions with other cellular macromolecules leading to the formation of cross-linked products. We synthesized and structurally characterized *N*-acetylcysteine cross-links formed in the reactions with aldehydic adducts of adenine nucleosides, which possess enol functionality and represent model α,β-unsaturated carbonyl systems. Studies performed by the use of NMR spectroscopy, DFT and *ab initio* methods established that two of these cross-links exist as rotamers stable at room temperature. Application of Atoms in Molecules Theory enabled hydrogen bonding and other stabilizing interactions within the studied molecules to be estimated. Under physiological conditions the cross-links were found to be relatively stable until N^{α}-acetyllysine was present in the reaction medium. The presence of this amino acid caused fast transformation of the *N*-acetylcysteine cross-links into a range of their lysine derivatives. Although instability of the cysteine adduct with acrolein was reported, we showed that the mechanism involved in the gradual decomposition of the *N*-acetylcysteine cross-links differs from that proposed for acrolein adduct degradation. This demonstrates that in spite of similarities in their structures, numerous α,β-unsaturated carbonyl compounds can interact with nucleophilic biomolecules by different mechanisms leading to structural heterogeneity of the resulting products. Our findings provide an explanation for difficulties in identifying the cysteine containing DPCs *in vivo* and *in vitro*, and may be of great importance with respect to detection and isolation of such lesions from biological materials.

Received 21st January 2017,
Accepted 16th February 2017

DOI: 10.1039/c7nj00270j

rsc.li/njc

Introduction

DNA–protein cross-links (DPCs) are bulky lesions formed when cellular proteins bind covalently to DNA. These lesions distort the DNA helix and can disturb normal DNA–protein interactions leading to impairment of DNA-involving processes such as transcription, replication, repair, recombination and chromatin remodeling.[1–3] RNA, due to its structural likeness to DNA, is presumed to exhibit similar reactivity towards protein cross-link formation. RNA–protein cross-links can interfere with processes related to both mRNA and noncoding RNA.[4–6] The location of cross-linking on the DNA constituent was found to influence the biological outcomes of DPC formation.[7,8] However the biological consequences of DPC formation depend not only on the DNA sequence involved in these lesions, but in a large part, on the protein trapped in it. While early reports suggested that only DNA-binding proteins can undergo crosslinking to DNA, recent studies have implied that any protein can be involved in DPC formation.[9,10]

Proteins related to a number of cellular processes were found to form DPCs. Among them are DNA replication and repair proteins,[3,11] architectural, structural and associated proteins, cell cycle proteins and chromatin regulators, proteins responsible for cellular homeostasis and stress response, transcription regulators and RNA splicing components.[3,12,13,14–17] In model reactions, lysozyme and serum albumin were also shown to undergo crosslinking to DNA.[10,18] Different proteins favor the formation of DPCs with specified DNA sequences.[2]

DPCs can be induced by exposure to a broad range of environmental agents but also by bifunctional electrophiles of endogenous origin which can react with a nucleophilic site on both DNA and amino acid side chains. Among such electrophiles, α,β-unsaturated carbonyl compounds and 2-oxoaldehydes such as glyoxal and methylglyoxal are known to induce DPCs.[9,19] Lysine, arginine, cysteine, histidine, and serine were found to form DPCs.[1,2,10] Nevertheless, the majority of reports refer

Adam Mickiewicz University in Poznań, Faculty of Chemistry, Umultowska 89b, 61-614 Poznań, Poland. E-mail: donatap@amu.edu.pl

† Electronic supplementary information (ESI) available. See DOI: 10.1039/c7nj00270j

mainly to the N-terminal and lysine side chain amino groups and to the guanidine group as protein structure fragments involved in such lesions. The cysteine residue thiol groups are the most nucleophilic sites in proteins, however the content of these residues in protein surfaces is much lower than those of other amino acids. Moreover cysteine containing DPCs were reported to be less stable than other types of such lesions.[10,11] Therefore studies on cysteine DPCs seem to be challenging.

Bis-electrophiles such as 1,2,3,4-diepoxybutane, the key carcinogenic metabolite of 1,3-butadiene and *N*,*N*-bis-(2-chloroethyl)-phosphorodiamidic acid as well as *N*,*N*-bis-(2-chloroethyl)-amine, the metabolites of cyclophosphamide used to treat some kinds of cancer and autoimmune diseases, have been shown to induce the formation of cysteine containing DPCs.[14–17,20–22]

The lipid peroxidation product, 4-hydoxy-2-nonenal, was demonstrated to modify an active site cysteine residue of protein disulfide isomerase which participates in the maturation of newly synthesized proteins through promoting correct disulfide formation.[23]

Another α,β-unsaturated aldehyde, acrolein, was found to be responsible for inactivation of protein tyrosine phosphatase 1B by binding covalently to the catalytic cysteine residue at the enzyme active site.[24]

Cysteine was also, besides lysine, shown to be involved in the DPCs formed by methylglyoxal between dG in the substrate DNA and the exonuclease deficient Klenow fragment of *E. coli* DNA polymerase I.[11] It was found that the yield of the cysteine cross-link was much lower than that of the lysine one, however, the chemical nature of the cross-linked compounds was not determined.[11] Glyoxal was also shown to induce the formation of these kinds of cross-links but the aldehyde was found to be a less potent crosslinking agent than methylglyoxal.[11] Although DNA–protein crosslinking activity of methylglyoxal was examined in a later study,[25] only the structure of the aldehyde cross-link between dG and N^{α}-acetyllysine was established.[25]

DPCs can be potentially used in biochemistry and medicine as biomarkers of oxidative/carbonyl stress and of chemical exposure.[2] Moreover, controlled formation of DPCs *in vitro* is a useful tool in proteomics analysis.[26,27] Therefore there is a great need for studies aimed at structure determination, formation mechanism elucidation and stability investigation of cysteine containing DPCs.

Recently, we found that aldehydic adducts of adenine nucleosides[28,29] (Fig. 1) exhibit potent cross-linking activity.[30] We showed that these adducts induce the formation of a range of cross-links while incubating with N^{α}- and N^{ε}-acetyllysine respectively.[30] The enol form predominates for dialdehyde functionality of the adducts in aqueous solution, therefore these chemicals represent model systems suitable for studies on α,β-unsaturated carbonyl compound cross-linking activity. In the present work we used these systems to study their reactivity toward *N*-acetylcysteine and we identified a range of cross-linked products. Our findings provide insight into the probable structures and stability of similar modifications potentially formed *in vivo*. They also clearly show that difficulties in identification and structural characterization of cysteine cross-links may result from their instability.

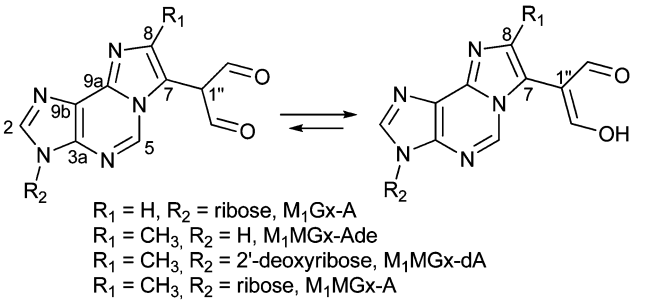

Fig. 1 Structures of the studied adducts: **M_1Gx-A**, **M_1MGx-Ade**, **M_1MGx-dA** and **M_1MGx-A**.[29]

Results and discussion

Reactions of M_1Gx-A with *N*-acetylcysteine

M_1Gx-A was synthesized as described previously[28] (Scheme 1) and subjected to reaction with *N*-acetylcysteine (NAC) in 0.1 M phosphate buffer (PB) solution at 37 and at 50 °C, respectively, for 10 days. LC-DAD analyses of the reaction mixtures revealed the presence of one major product named **M_1Gx-A-NAC** (Fig. 2), which achieved maximum concentration after 36 h of heating at 50 °C.

Formation of this product was also observed at 37 °C, however, at this temperature the yield of **M_1Gx-A-NAC** was lower. The UV spectrum of this compound exhibited absorption maxima at λ = 234 and λ = 300 nm, and an absorption minimum at λ = 260 nm (Fig. 3).

Structural data provided by mass spectrometry (*m*/*z* 507 $[M + H]^+$, ESI,† Fig. S7) indicated that **M_1Gx-A-NAC** is composed of one *N*-acetylcysteine molecule and one **M_1Gx-A** molecule. A spectrum resulting from MS/MS analysis, besides the molecular ion signal, showed two fragment ion signals at *m*/*z* 375 and 246 (ESI,† Fig. S8). The former signal corresponded to the neutral

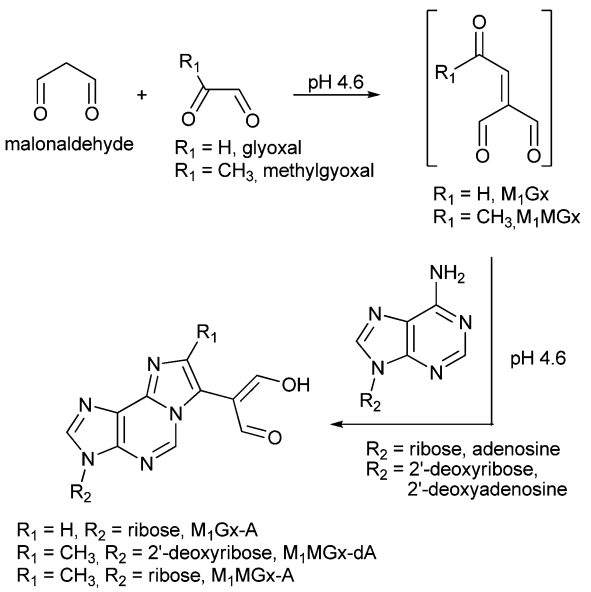

Scheme 1 Formation of malonaldehyde-glyoxal and malonaldehyde-methylglyoxal adducts of adenine nucleosides.

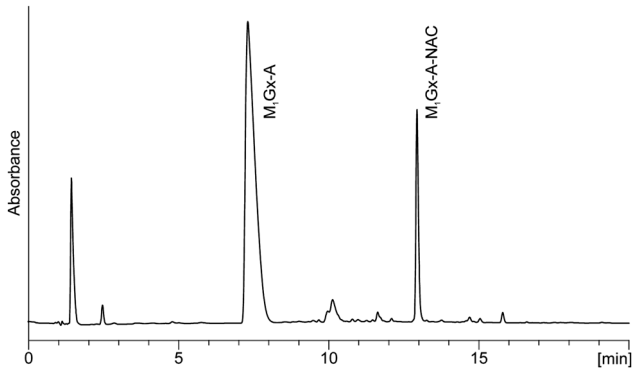

Fig. 2 C18 analytical column LC-DAD chromatogram (recorded at λ = 254 nm) of **M_1Gx-A** with *N*-acetylcysteine reaction mixture held in 0.1 M phosphate buffer solution at 50 °C for 36 h.

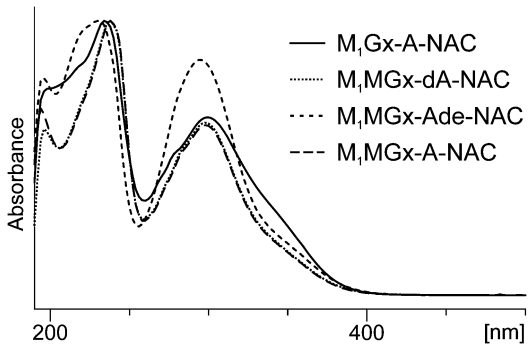

Fig. 3 UV-Vis spectra of *N*-acetylcysteine cross-links recorded with a diode array detector as the compounds eluted from the column. (For analysis conditions see the Experimental section.)

loss of a ribosyl unit, and the latter resulted from the neutral loss of a ribosyl unit and cleavage of the bond between the sulfur atom and β-carbon atom in the *N*-acetylcysteine residue (Fig. 4 and ESI,† Fig. S8).

For definitive structural characterization of **M_1Gx-A-NAC** a preparative scale reaction was performed, and the major product was isolated (13 mg, 25% yield) and subjected to spectroscopic studies. The data obtained from the **M_1Gx-A-NAC** NMR spectra (ESI,† Fig. S43–S48) are presented in Table 1 and in part in Fig. 5.

The singlet one-proton signal observed in the ^{1}H NMR spectrum at 9.52 ppm was assigned to the aldehyde proton based on the chemical shift and ^{1}H-^{13}C correlation with the carbon atom signal at 194.12 ppm. The presence of one aldehyde proton suggested that *N*-acetylcysteine was attached to the adduct aldehydic functionality. In the ^{13}C NMR spectrum the signal appearing at 119.23 ppm arose from the atom not bonded to the proton and was assigned to the C1″ carbon atom. The structure proposed for **M_1Gx-A-NAC** (Fig. 6) was confirmed by correlations observed in the HMBC spectrum (Table 1).

Reactions of M_1MGx-dA with *N*-acetylcysteine

M_1MGx-dA and **NAC** were held in 0.1 M and 1 M PB solutions at 37 and 50 °C, respectively, for 14 days. The pH of the reaction mixtures was monitored and it was found to be 7.4 for 1 M, and 3 for 0.1 M PB solution. The reaction mixture chromatograms derived from LC-DAD analyses showed the presence of two major products (**M_1MGx-Ade–NAC** and **M_1MGx-dA–NAC**) in 0.1 M PB solution (Fig. 7) and one major product (**M_1MGx-dA–NAC**) in 1 M PB solution (data not shown).

The compounds exhibited very similar UV spectra (**M_1MGx-Ade–NAC**: λ_{max} = 232, 296 nm, λ_{min} = 256 nm; **M_1MGx-dA–NAC**: λ_{max} = 238, 298 nm, λ_{min} = 260 nm) (Fig. 3). The mass spectrum of **M_1MGx-Ade–NAC** displayed a signal at *m*/*z* 389 $[M + H]^+$ (ESI,† Fig. S10), while the spectrum of **M_1MGx-dA–NAC** revealed a signal at *m*/*z* 505 $[M + H]^+$ (ESI,† Fig. S14). Data derived from the UV and mass spectra (ESI,† Fig. S10–S17) of **M_1MGx-Ade–NAC** and **M_1MGx-dA–NAC** indicated that both compounds were structural analogues which differ only in the presence of a 2′-deoxyribosyl unit. Formation of adenine derivative can be explained by hydrolysis of *N*-glycosidic

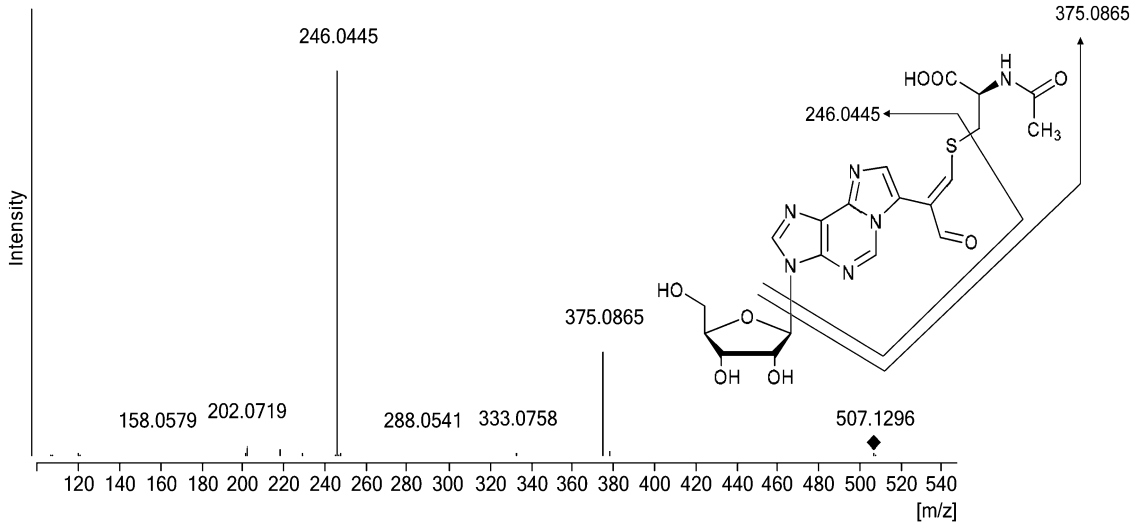

Fig. 4 Representative MS/MS trace for the synthesized cross-link; the positive ion MS/MS spectrum of **M_1Gx-A-NAC** (collision energy 30 eV).

Table 1 NMR data of **M_1Gx-A-NAC** (D_2O)

	δ(H) [ppm]	Multiplicity	$J_{H,H}$ [Hz]	δ(C) [ppm]	HMBC	NOESY
H–C1′	6.21	d	5.43	91.29	C2, C3a, C2′, C3′, C4′	H–C2, H–C2′, H–C3′, H–C4′
H–C2′	4.86	m		76.84	C1′	H–C2, H–C1′, H–C3′, Ha–C5′
H–C3′	4.50	m		73.25	C1′, C5′	H–C2, H–C1′, H–C2′, Ha–C5′, Hb–C5′
H–C4′	4.30	dd	4.12; 7.34	88.29	C1′, C2′, C3′, C5′	H–C1′, Ha–C5′, Hb–C5′
Ha–C5′	3.88	dd	3.88; 12.72	64.25	C3′, C4′	H–C2′, H–C3′, H–C4′, Hb–C5′, H–C2
Hb–C5′	3.95	dd	3.04; 12.73		C3′, C4′	H–C3′, H–C4′, Ha–C5′
H–C2	8.49	s		143.95	C3a, C9b, C1′	H–C1′, H–C2′, H–C3′, Ha–C5′
C3a				141.67		
H–C5	8.63	s		139.51	C3a, C7, C9a, C9b	Ha–Cβ
C7				119.23		
H–C8	7.69	s		137.57	C7, C9a, C1″, C2″	CH_3
C9a				144.45		
C9b				125.60		
C1″				127.63		
H–C2″	8.66			170.62	C7, CHO, C1″, Cβ	CHO, Ha–Cβ, Hb–Cβ, H–Cα
CHO	9.52	s		194.12	C7, C1″, C2″	H–C2″
H–Cα	4.57	dd	4.33, 7.79	57.68	Cβ, COOH, C═O (Ac)	H–C2″, Ha–Cβ, Hb–Cβ
Ha–Cβ	3.42	dd	7.83, 14.18	40.65	Cα, C2″, COOH	H–Cα, Hb–Cβ, H–C2″
Hb–Cβ	3.61	dd	4.33, 14.19		Cα, C2″, COOH	H–Cα, Ha–Cβ, H–C2″
COOH				178.30		
C═O (Ac)				176.58		
CH_3 (Ac)	2.05			24.86	C═O (Ac), Cα, Cβ	H–C8

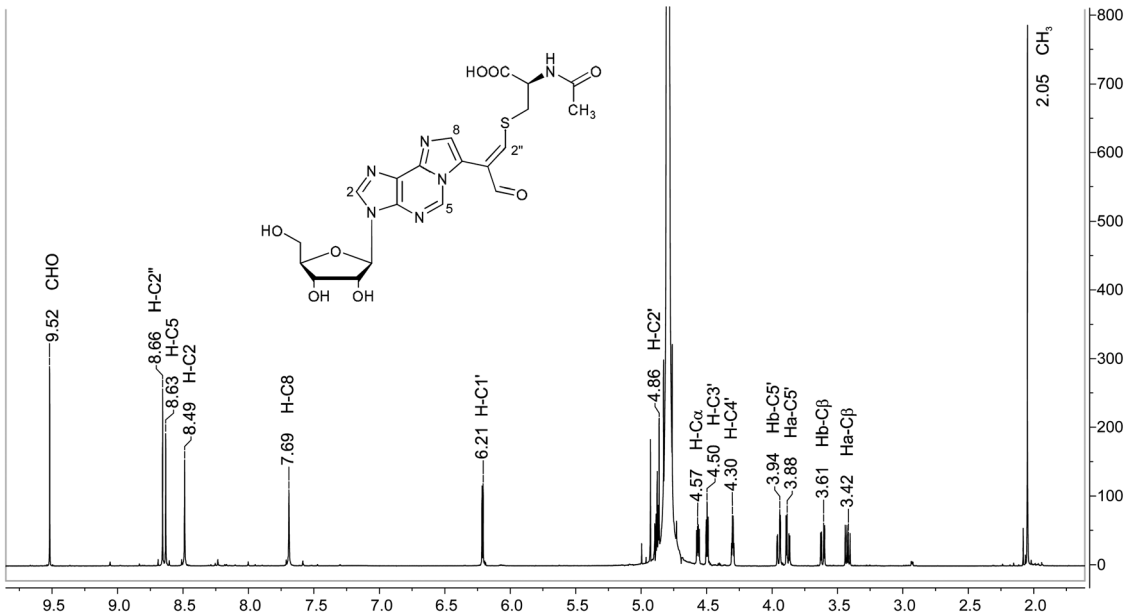

Fig. 5 Representative NMR spectrum of the synthesized cross-link; ^{1}H NMR spectrum of **M_1Gx-A-NAC** (D_2O).

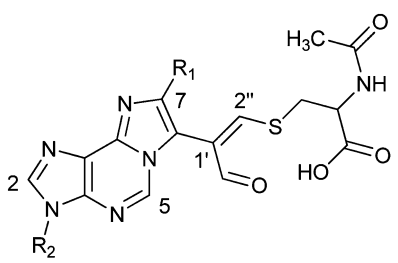

Fig. 6 Structures proposed for the cross-links: **M_1Gx-A-NAC**, **M_1MGx-Ade–NAC** and **M_1MGx-A-NAC**.

bond in the initially formed cross-link and in **M_1MGx-dA**. Moreover, these data suggested that **M_1MGx-Ade–NAC** and **M_1MGx-dA–NAC** consisted of one molecule of *N*-acetylcysteine and one molecule of the adduct. The isolated **M_1MGx-Ade–NAC** (9 mm, 30% yield) was subjected to spectroscopic studies which confirmed the structure proposed for the compound as shown in Fig. 6. The HMBC spectrum of **M_1MGx-Ade–NAC** exhibited analogous correlations with the HMBC spectrum of **M_1Gx-A-NAC**. (For detailed NMR data see the ESI,† Table S1 and Fig. S49–S53.)

Reaction of M_1MGx-A with *N*-acetylcysteine

Due to the instability of **M_1MGx-dA** under reaction conditions the adenosine analogue of this adduct (**M_1MGx-A**) was used to

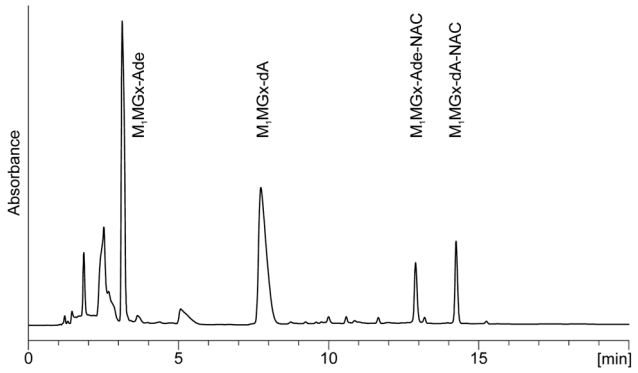

Fig. 7 C18 analytical column LC-DAD chromatogram (recorded at 254 nm) of **M_1MGx-dA** with NAC reaction mixture held in 0.1 M PB solution at 37 °C for 3 h.

study its reactivity towards NAC. In the reaction performed in 0.1 M PB solution at 50 °C one major product (**M_1MGx-A-NAC**) was formed (ESI,† Fig. S1). The compound exhibited a very similar UV spectrum (λ_{max} = 238, 298 nm and λ_{min} = 260 nm) to the UV spectra of **M_1Gx-A-NAC**, **M_1MGx-dA–NAC** and **M_1MGx-Ade–NAC** (Fig. 3). Data derived from the mass spectrum (*m*/*z* 521 $[M + H]^+$, (ESI,† Fig. S18)) suggested that the product was a structural analogue of the compounds formed in the reaction of **M_1MGx-dA** with NAC. However, contrary to the reaction with **M_1MGx-dA**, no hydrolysis of the *N*-glycosidic bond in the forming product was observed. The spectrum derived from the **M_1MGx-A-NAC** MS/MS analysis showed fragmentation similar to that observed for **M_1Gx-A-NAC**. Besides the molecular ion signals, two fragment ion peaks at *m*/*z* 389 and 260 were present in the spectrum (ESI,† Fig. S19). The former corresponded to the neutral loss of a ribosyl unit, and the latter resulted from the neutral loss of a ribosyl unit and cleavage of the bond between the sulfur atom and β-carbon atom in the *N*-acetylcysteine residue.

The preparative scale reaction of **M_1MGx-A** with **NAC** was performed and **M_1MGx-A-NAC** was isolated (22 mg, 28% yield) for structural studies (Table 2 and ESI,† Fig. S54–S59). The correlations observed in the HMBC spectrum were crucial for **M_1MGx-A-NAC** structure determination.

Mechanism of the *N*-acetylcysteine cross-link formation

M_1Gx-A-NAC, **M_1MGx-Ade–NAC** and **M_1MGx-A-NAC** are structural analogues of the cross-links of the aldehydic adenine nucleosides adducts with lysine derivatives previously identified in our laboratory.[30] Therefore the mechanism proposed for lysine cross-linked product formation is most likely valid also for giving rise to the *N*-acetylcysteine modification. This mechanism involves Michael addition of the amino acid thiol group to the adducts' α,β-unsaturated aldehydic functionality, followed by dehydration (Scheme 2) and is in agreement with the well-known rule that for soft nucleophiles such as thiol groups, conjugate addition is a typical reaction with α,β-unsaturated carbonyls.

N-Acetylcysteine cross-link stability

To determine the stability of the *N*-acetylcysteine cross-links under physiological conditions pure **M_1Gx-A-NAC**, **M_1MGx-Ade–NAC** and **M_1MGx-A-NAC** were dissolved separately in 0.1 M PB solution (pH 7.4) and stored at 37 °C for 30 days. The compounds' stability was monitored by using LC and LC-MS systems with diode array detection. **M_1Gx-A-NAC**, **M_1MGx-Ade–NAC** and **M_1MGx-A-NAC** were found to be relatively stable under the applied conditions with half-life times above 20 days. The cross-links underwent slow degradation forming two products (Fig. 8 and ESI,† Fig. S2 and S3).

On the basis of mass and UV spectra, and co-elution with the appropriate adducts used as reference compounds, the products eluted at 8.5 min (Fig. 8), and at 2.7 and 6.2 min (ESI,† Fig. S2 and S3) were identified as the substrate adducts: **M_1Gx-A,**

Table 2 NMR data of **M_1MGx-A-NAC** derived from spectra recorded in D_2O

	δ(H) [ppm]	Multiplicity	$J_{H,H}$ [Hz]	δ(C) [ppm]	HMBC	NOESY
H–C1′	6.20	d	5.44	91.79	C2, C3a, C2′, C3′, C4′	H–C2, H–C2′, H–C3′, H–C4′
H–C2′	4.87	dd	5.13; 10.18	76.81	C1′	H–C2, H–C1′, H–C3′, Ha–C5′, Hb–C5′
H–C3′	4.50	m		73.31	C1′, C5′	H–C2, H–C1′, H–C2′, Ha–C5′, Hb–C5′
H–C4′	4.30	dd	3.67; 7.49	88.35	C1′, C2′, C3′, C5′	H–C1′, Ha–C5′, Hb–C5′
Ha–C5	3.90	dd	4.26; 12.69	64.31	C3′, C4′	H–C2′, H–C3′, H–C4′, Hb–C5′, H–C2
Hb–C5′	3.94	dd	3.06; 12.71		C3′, C4′	H–C2′, H–C3′, H–C4′, Ha–C5′
H–C2	8.49	s (split)		144.13	C3a, C9b, C1′	H–C1′, H–C2′, H–C3′, Ha–C5′
C3a				141.98		
H–C5	8.55	s (split)		138.75	C3a, C7, C9a, C9b	
C7				115.30		
C8				145.10		
C9a				143.75		
C9b				124.83		
CH_3	2.32	s (split)		15.63	C7, C8, C1″, C2″, CHO	CHO, C2″, Hb–Cβ
C1″				127.27		
H–C2″	8.74	s (split)		171.54	C7, CHO, Cβ	
CHO	9.57	s		193.25	C7, C8, C1″, C2″	H–C2″, CH_3 (Ac)
H–Cα	4.59	dd (split)	4.30; 8.37	57.68	Cβ, C═O (Ac)	H–C2″, Ha–Cβ, Hb–Cβ, CH_3 (Ac)
Ha–Cβ	3.41	dd (split)	8.34; 14.24	40.37	Cα, C1″, C2″, COOH	H–Cα, Hb–Cβ, H–C2″
Hb–Cβ	3.66	dd (split)	4.29; 13.96		Cα, C1″, C2″, COOH	H–Cα, Ha–Cβ, H–C2″, CH_3
COOH				178.29		
C═O (Ac)				175.58		
CH_3 (Ac)	2.08	s (split)		24.90	C═O (Ac)	H–C2″, CHO, H–Cα

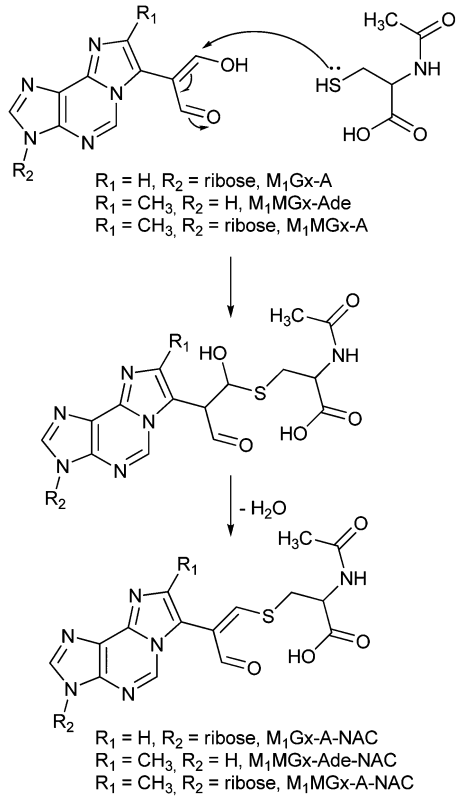

Scheme 2 Proposed mechanism of *N*-acetylcysteine cross-link formation.

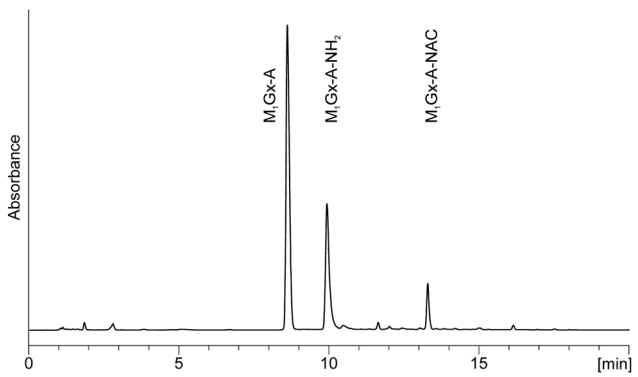

Fig. 8 C18 analytical column LC-DAD chromatogram (recorded at 254 nm) of the 0.1 M PB solution of **M_1Gx-A-NAC** held at 37 °C for 17 days.

M_1MGx-Ade and **M_1MGx-A**, respectively. Compounds with longer retention times (Fig. 8 and ESI,† Fig. S2 and S3) exhibited almost identical UV spectra with λ_{max} at 236 and 272 nm and λ_{min} at 256 nm (Fig. 9). Spectrometric studies were performed and the compounds were found to give rise to protonated molecular ion signals recorded at *m*/*z* 361, 243 and 375, respectively (ESI,† Fig. S22, S26 and S30). The corresponding substrate adduct **M_1Gx-A**, **M_1MGx-Ade** and **M_1MGx-A** ion signals were recorded at *m*/*z* 362, 244 and 376, respectively (ESI,† Fig. S20, S24 and S28). Such small differences between the appropriate values were very surprising and prompted us to perform ESI-MS/MS analyses using high collision energy for the degradation product derived

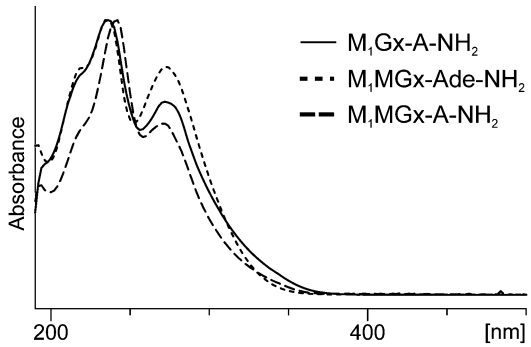

Fig. 9 UV-Vis spectra of *N*-acetylcysteine cross-link degradation products: **M_1Gx-A-NH_2**, **M_1MGx-Ade-NH_2** and **M_1MGx-A-NH_2** recorded with a diode array detector as the compounds eluted from the column. (For analysis conditions see the Experimental section.)

from **M_1MGx-Ade–NAC** and for **M_1MGx-Ade**. The resulting spectra showed a range of signals arising from similar fragmentation ions (ESI,† Fig. S25 and S27). In the mass spectrum of **M_1MGx-Ade** the signal appearing at *m*/*z* 226 corresponded to the neutral loss of water molecules ($[M–H_2O + H]^+$, ESI,† Fig. S25). In the mass spectrum of the **M_1MGx-Ade–NAC** degradation product, the signal recorded at *m*/*z* 226 was attributed to the neutral loss of an ammonia molecule ($[M–NH_3 + H]^+$, ESI,† Fig. S27). Moreover the UV spectra of the degradation products resembled those of cross-links arising from reactions of the aldehydic adducts of adenine nucleosides with N^{α}-acetyllysine[30] (Fig. 9 and 10).

In these cross-links the free amino group of N^{α}-acetyllysine is attached to the adducts' carbonyl carbon atom (Fig. 11B). Based on all these findings we concluded that the degradation products of *N*-acetylcysteine cross-links represent structures depicted as shown in Fig. 11A.

The mechanism responsible for the formation of these products is not clear, however it seems to be likely that they arise from 1,4-addition of ammonia to the cross-link carbon atom C-2″. Ammonium bicarbonate solution used for isolation and purification of the cross-links is a probable source of ammonia. Although the fractions containing the cross-links devoted to stability studies were evaporated to dryness, the obtained residues might contain ammonia in sufficient amounts for nucleophilic attack.

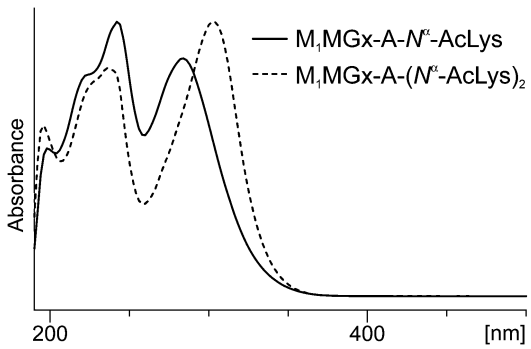

Fig. 10 UV-Vis spectra of products formed in the mixture of **M_1MGx-A-NAC** with N^{α}-acetyllysine. The spectra were recorded with a diode array detector as the compounds eluted from the column.

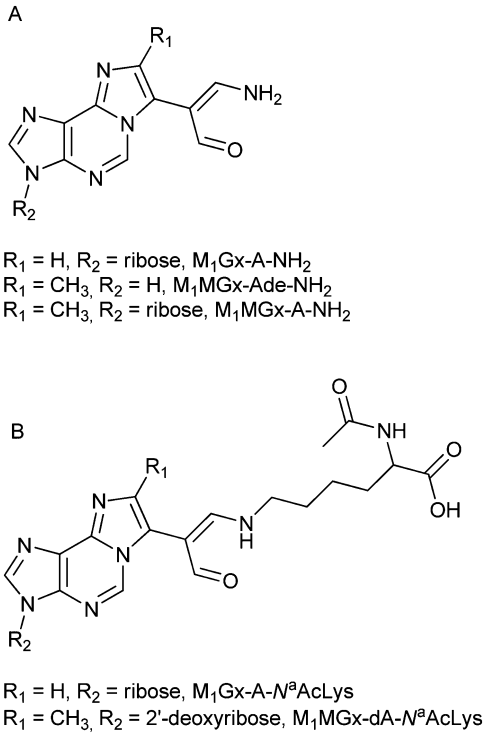

Fig. 11 Proposed structures of **M_1MGx-Ade–NAC**, **M_1MGx-A-NAC** and **M_1MGx-A-NAC** degradation products (A), and of known N^{α}-acetyllysine cross-links with the studied adducts[21] (B).

Ammonia could also arise from non-enzymatic oxidation of amino acids[31,32] released from the cross-links. The results derived from stability studies of the *N*-acetylcysteine cross-links performed in the presence of N^{α}-acetyllysine provide support for a Michael addition of ammonia being involved in the cross-link degradation product formation. These results are also in good agreement with the literature data suggesting that cysteine containing DPCs are less stable than DPCs in which other amino acids are involved.[10]

N-Acetylcysteine cross-link stability in the presence of N^{α}-acetyllysine

M_1Gx-A-NAC and **M_1MGx-A-NAC** were found to be much more unstable while incubating at 37 °C with N^{α}-acetyllysine. The half-life time of the cross-links decreased to a few hours. LC-DAD analyses of the reaction mixtures revealed the formation of two products (Fig. 12 and ESI,† Fig. S4). On the basis of mass and UV spectra the compounds were identified as the 1 : 2 and 1 : 1 cross-linked products of **M_1Gx-A** and **M_1MGx-A** with N^{α}-acetyllysine previously characterized in our laboratory.[30]

Cai *et al.*[33] examined the reactivity of acrolein towards model peptides containing cysteine, lysine and histidine, and found that in the initial step the reaction pathway involves a Michael addition of the cysteine thiol group. Due to the loss of electron donation from the double C=C bond, the aldehyde group in the resulting adduct is more electrophilic than in acrolein and reacts with an amino group forming a Schiff base adduct. This adduct can undergo rearrangement through an intermediate

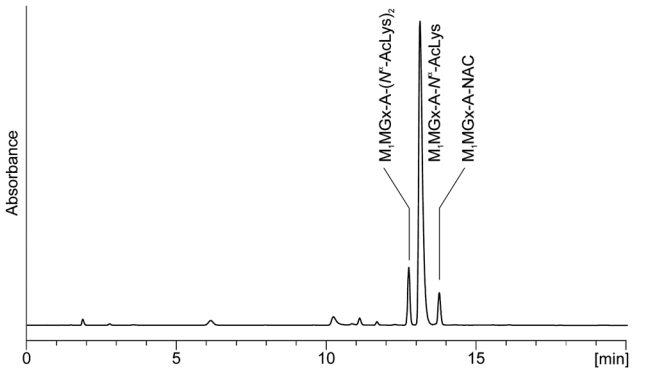

Fig. 12 C18 analytical column LC-DAD chromatogram (recorded at 254 nm) of the **M_1MGx-A-NAC** mixture with N^{α}-acetyllysine held in 0.1 M PB solution at 37 °C for 1 day.

enamine to a more stable Schiff base adduct which contains a C=C bond conjugated with the imine group (Scheme 3).[33]

This mechanism cannot be involved in the transformation of **M_1Gx-A-NAC** and **M_1MGx-A-NAC** into the N^{α}-acetyllysine cross-linked products. The *N*-acetylcysteine derivatives possess substituted α,β-unsaturated aldehydic functionality and therefore are unable to form an enamine intermediate. In the reactions of **M_1Gx-A** and **M_1MGx-A** with N^{α}-acetyllysine, apart from cross-links resulting from Michael addition also imine-enamine adducts containing two amino acid residues were formed.[30] These adducts arose from 1,2-addition of the N^{α}-acetyllysine amino group to the initially formed Michael addition products, the enamine cross-links, followed by dehydration.[30] The imine–enamine adducts are stabilized by a hydrogen bond between the imine nitrogen atom and the proton of the enamine N–H group.[30] Such stabilization would not be possible in the products resulting from 1,2-addition of N^{α}-acetyllysine to **M_1Gx-A-NAC** and **M_1MGx-A-NAC** and consequently formation of such compounds was not observed.

In light of these data we proposed that the mechanistic explanation for the transformation of **M_1Gx-A-NAC** and **M_1MGx-A-NAC** into 1 : 1 cross-linked products of **M_1Gx-A** and **M_1MGx-A** with N^{α}-acetyllysine is based on a Michael addition of N^{α}-acetyllysine to the *N*-acetylcysteine cross-links in conjunction with *N*-acetylcysteine elimination (Scheme 4). Formation of 1 : 2 cross-links occurs as previously described.[30]

To provide additional support for the proposed mechanism, studies on **M_1Gx-A** and **M_1MGx-A** reactivity towards an *N*-acetylcysteine and N^{α}-acetyllysine mixture were performed.

M_1Gx-A and M_1MGx-A reactivity towards a mixture of *N*-acetylcysteine and N^{α}-acetyllysine

M_1Gx-A and **M_1MGx-A** were separately subjected to simultaneous reactions with *N*-acetylcysteine and N^{α}-acetyllysine. LC-DAD and LC-MS analyses revealed that **M_1Gx-A-NAC** and **M_1MGx-A-NAC** were initially formed cross-linked products (ESI,† Fig. S5 and S6). Prolonged reactions led to gradual decline in the amount of *N*-acetylcysteine cross-links and to the formation of N^{α}-acetyllysine derivatives which became the main products of the reactions.

For the purpose of estimating the difference in energy between the *N*-acetylcysteine and N^{α}-acetyllysine cross-links,

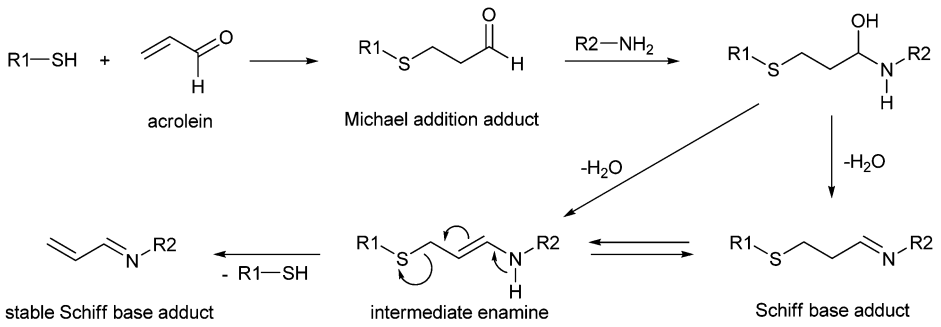

Scheme 3 Formation of adducts in the reaction of model peptides with acrolein.[33]

quantum-chemical investigations using isodesmic model systems were performed. The obtained results showed that the energy of the compound formed by amino group addition is lower than that of the product arising from thiol group addition (Fig. 13). ΔE calculated at the M06/6-311++G(2df,2pd) and M06/aug-cc-pVDZ levels was equal to 4.4 and 5.5 kcal mol^{-1}, respectively, indicating that, in accordance with the experimental data, N^{α}-acetyllysine cross-links are more stable than their *N*-acetylcysteine derivatives.

Variable-temperature ^{1}H NMR studies on M_1MGx-Ade–NAC and M_1MGx-A-NAC

^{1}H NMR spectra of **M_1MGx-Ade–NAC** and **M_1MGx-A-NAC** recorded at room temperature exhibited doubling of signals (ESI,† Fig. S49 and S54). This phenomenon was also observed in the ^{13}C NMR spectra of both cross-links (ESI,† Fig. S50 and S55). However not all of the carbon and proton signals were duplicated. A very intriguing fact was that no duplication of signals was seen in the spectra of **M_1Gx-A-NAC** (ESI,† Fig. S43 and S44). The three cross-linked products differ only in the substituent at C8; the proton attached to C8 in **M_1Gx-A-NAC** is replaced in **M_1MGx-Ade–NAC** and **M_1MGx-A-NAC** with a methyl group. The presence of this group was supposed to cause hindered rotation over the C7–C1″ bond resulting in the existence of two rotational conformers (rotamers). To confirm this hypothesis, variable-temperature ^{1}H NMR studies together with computational investigations were performed.

The pattern of signal duplication in the ^{1}H NMR spectrum of **M_1MGx-Ade–NAC** (D_2O) suggested that at 297 K the cross-link existed as two rotamers (A and B) separated by a rotational energy barrier around the C7–C1″ bond sufficiently high to prevent fast interconversion of these conformers at room temperature. Both rotamers were detected by the use of signals at 1.96 ppm assigned to methyl protons of the acetyl group as a marker (Fig. 14).

At 297 K the signals appeared as a split singlet due to the existence of the two rotamers in the ratio of 1.44 : 1.56. The concentration of both conformers was P_A = 0.48 and P_B = 0.52. The frequency difference, $\Delta\nu$, between the methyl proton signals was 8.42 Hz. This value increased to 8.52 Hz when the sample was cooled to 286 K, but reheating to room temperature resulted in the return to the initial $\Delta\nu$ value. As the temperature increased the signals for the two rotamers were still detected, although within particular pairs, the signals broadened and moved closer together. The two signals coalesced to a single one which appeared at 2.63 ppm in the spectrum measured at 371.5 K (T_c) (Fig. 14). The other pairs of signals coalesced at lower temperatures.

The Gibbs free energy of activation for interconversion between the two rotamers was calculated on the basis of NMR studies using Earing's equations modified by Shanan-Atidi and Bar-Eli:[34]

$$\Delta G_A^{\ddagger} = 4.57T_c\{10.62 + \log[X/2\pi(1 - \Delta P)] + \log(T_c/\Delta\nu)\}$$

$$\Delta G_B^{\ddagger} = 4.57T_c\{10.62 + \log[X/2\pi(1 + \Delta P)] + \log(T_c/\Delta\nu)\}$$

X was obtained by use of the following equation:[34]

$$P_A - P_B = \Delta P = [(X^2 - 2)/3]^{3/2} \times 1/X$$

For ΔP = 0.04 the X value is equal to 1.636.

The free energy of rotamer A activation was $\Delta G_A^{\ddagger}$ = 19.97 kcal mol^{-1}, and for rotamer B $\Delta G_B^{\ddagger}$ = 19.85 kcal mol^{-1}.

The high temperature caused partial decomposition of the studied compound and formation of degradation products being a source of additional signals in the ^{1}H NMR spectra.

Analogous variable-temperature ^{1}H NMR studies were also performed for **M_1MGx-A-NAC** (D_2O). The acetyl methyl proton signals which appeared at 1.96 ppm in the spectrum recorded at 279 K were again used as a marker. Two rotational conformers of the cross-link existed nearly in the same ratio as the rotamers of the adenosine analogue (1.43 : 1.57) (ESI,† Fig. S40). The frequency difference, $\Delta\nu$, between the marker signals was 9.48 Hz. The two signals coalesced to a single peak at 2.67 ppm in the spectrum recorded for the overheated sample at 375 K (T_c). At T_c the coalescence of the split signals was observed for the entire ^{1}H NMR spectrum, although the other pairs of signals coalesced at lower temperatures (ESI,† Fig. S40).

The Gibbs free energy of activation for rotamer A was 19.95 kcal mol^{-1}, and for rotamer B was 20.01 kcal mol^{-1}.

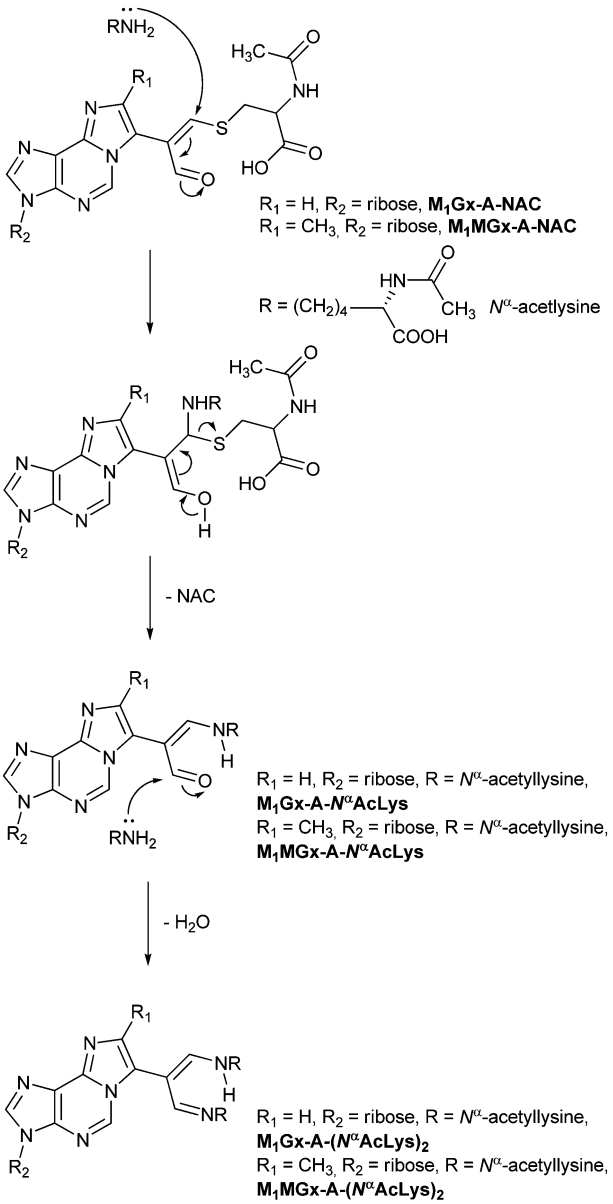

Scheme 4 Mechanism proposed for transformation of the cysteine cross-links into their N^{α}-acetyllysine derivatives.

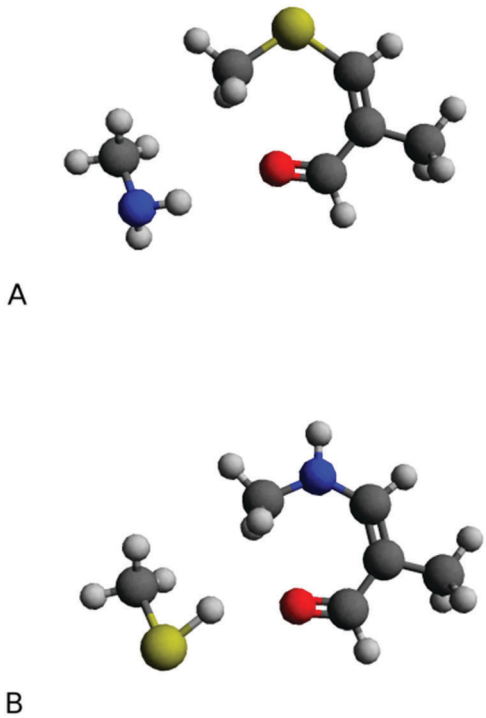

Fig. 13 Isodesmic models for cross-links: product resulting from thiol group addition (A), and compound arising from amino group addition (B). (Calculations performed at the M06/6-311++G(2df,2pd) level.)

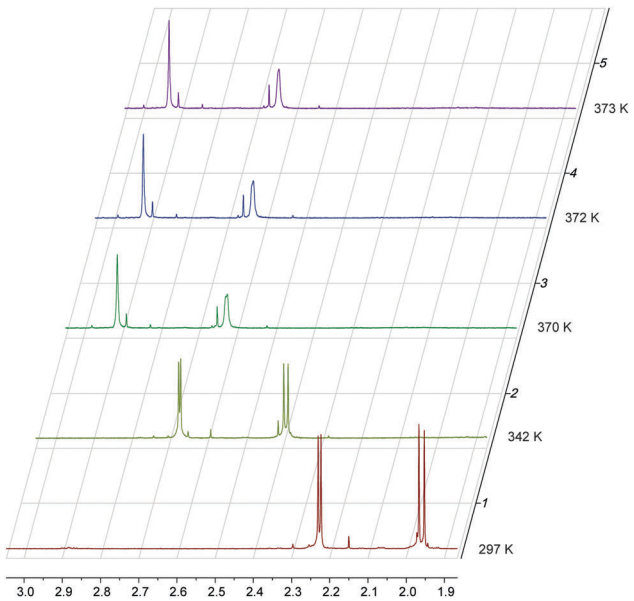

Fig. 14 Fragments of **M_1MGx-Ade–NAC** ^{1}H NMR spectra (D_2O) recorded at 297.2 K (1), 342.6 K (2), 370.4 K (3), 371.5 K (4) and 372.6 K (5). The split acetyl proton signals at 1.96 coalesced to a singlet at T_c = 371.5 K, and the methyl proton signals at 2.23 ppm coalesced at lower temperatures.

The almost identical values were in good agreement with the observation that in the ^{1}H NMR spectrum the paired signals appeared in a nearly 1 : 1 ratio.

Quantum-chemical studies on M_1MGx-Ade–NAC and M_1MGx-A-NAC rotamer interconversion

The aim of the quantum chemical investigations was to examine hindered rotation around the C7–C1″ bond in **M_1MGx-A-NAC** and **M_1MGx-Ade–NAC**. Rotation around this bond is associated with changes in the dihedral angle N6–C7–C1″–C2″ values and induces the molecules' helicity. *P* helicity corresponds to positive values of this angle, and *M* helicity to angles of negative values (Fig. 15). **TS_0** describes the transition state structure with the dihedral angle N6–C7–C1″–C2″ of about 0° (Fig. 16).

In this structure atoms within the N6–C7–C1″–C2″ fragment adopt synperiplanar geometry. In the transition state structure with the dihedral angle of about 180° (**TS_180**) atoms within the N6–C7–C1″–C2″ fragment adopt antiperiplanar geometry (Fig. 16). The studied molecules differ also in the conformation of the

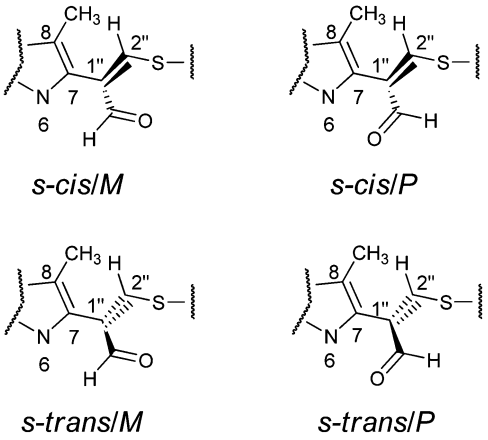

Fig. 15 The geometry of conformers in energy minima: s-*cis*/*M*, s-*cis*/*P*, s-*trans*/*M* and s-*trans*/*P*.

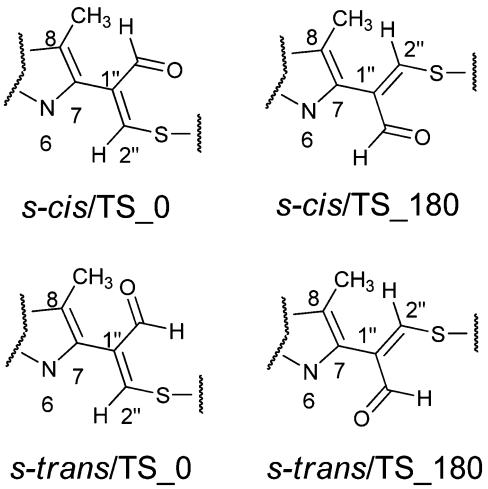

Fig. 16 The synperiplanar (**TS_0**) and antiperiplanar (**TS_180**) geometry of the transition states with appropriate conformation of the aldehyde group: s-*cis*/**TS_0**, s-*cis*/**TS_180**, s-*trans*/**TS_0** and s-*trans*/**TS_180**.

aldehyde group. This group exists in s-*cis* conformation when the dihedral angle O–CHO–C1″–C2″ adopts the value of about 0°, and possess s-*trans* conformation for this angle of about 180° (Fig. 15 and 16). The rotation of the aldehyde group occurs through transition state structures with dihedral angle O–CHO–C1″–C2″ values of about 90° (**TS_90**) and −90° (**TS_−90**).

Quantum-chemical studies *in vacuo* at the M06/6-31G(d) level of theory showed that the relative energies of the s-*trans* conformers of **M$_1$MGx-Ade–NAC** were generally slightly higher (about 1–4 kcal mol^{-1}) than the energies of the appropriate s-*cis* conformers (Chart 1). Only for N6–C7–C1″–C2″ dihedral angle values from −150° to −170° were the s-*trans* conformers energetically favorable (Chart 1).

Two energy minima were found for the s-*cis* conformers: for a structure with the N6–C7–C1″–C2″ dihedral angle value of −120.6° (minimum s-*cis*/*M*) and also of 130.8° (minimum s-*cis*/*P*) (Chart 1, Table 3 and Fig. 17).

The difference in the relative energy between these two minima was very small (0.85 kcal mol^{-1}). This fact was in good

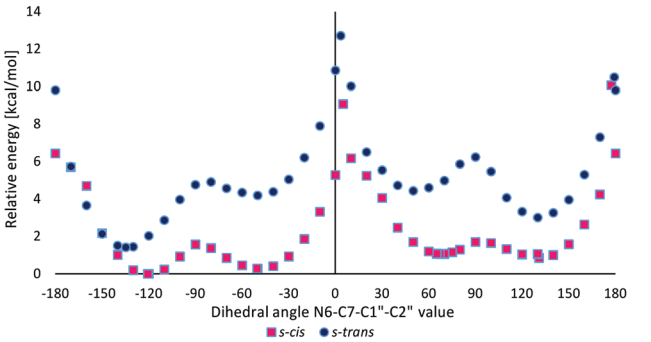

Chart 1 The relative energy of s-*cis* and s-*trans* conformers of **M$_1$MGx-Ade–NAC** dependent on the N6–C7–C1″–C2″ dihedral angle value calculated at the M06/6-31G(d) level of theory *in vacuo*.

agreement with experimental data which indicated that the two rotamers of **M$_1$MGx-Ade–NAC** existed in almost equal amounts. The energetically preferred transition state structure was found for s-*cis* conformers with the N6–C7–C1″–C2″ dihedral angle value of about 0° (s-*cis*/**TS_0**, Table 3). It was characterized by ΔE equal to 9.08 kcal mol^{-1}. The ΔE values of other transition state structures were slightly higher (up to 12.72 kcal mol^{-1}, Table 3). Application of thermal correction led to transition state structures with Gibbs free energies (ΔG) in the range of 11.73–14.45 kcal mol^{-1} being obtained (Table 3). To take into account the effect of solvent (water), the calculations were performed with the use of the polarizable continuum model (PCM). The obtained results were very similar to those received for the molecules *in vacuo* (Table 3). ΔE values calculated using the M06/6-31G(d) method did not differ significantly from the values obtained with larger basis sets (M06/6-31++G(d,p) and B3LYP/6-31++G(d,p)) (Table 4). Application of the atom–atom dispersion correction (ωB97X-D) led to slightly higher ΔE values compared to those obtained with the use of standard hybrid functionals (Table 4). The best correlation between the experimentally obtained rotational energy barrier and calculated ΔE values was only achieved using the MP2 perturbation method.

Quantum-chemical studies of rotation around the C7–C1″ bond in **M$_1$MGx-A-NAC** gave very similar results to those described for **M$_1$MGx-Ade–NAC** indicating that the presence of the ribosyl unit had no significant impact on the values of energy barriers between the **M$_1$MGx-A-NAC** conformers, nor on the ΔE values of conformers representing structures of transition states and minima found in the curves of relative energies as a function of the N6–C7–C1″–C2″ dihedral angle values (ESI,† Chart S2, Tables S3, S4 and Fig. S41).

Hydrogen bond formation in M$_1$MGx-Ade–NAC and M$_1$MGx-A-NAC based on atoms in molecules theory

Bader's atoms in molecules (AIM) theory[35] was applied in order to investigate the intramolecular hydrogen bond formation (or other stabilizing interactions) which may stabilize the rotamers' structures and inhibit their fast interconversion at room temperature.

The topological parameters, such as the electron density at bond critical points (BCPs), ρ_{BCP}, its Laplacian, $\nabla^2\rho_{BCP}$ and the

Table 3 Comparison of the relative energies (ΔE) and Gibbs free energies (ΔG) of s-*cis* and s-*trans* conformers of **M_1MGx-Ade–NAC** calculated at the M06/6-31G(d) level of theory *in vacuo* and using PCM for water

	In vacuo			PCM (water)		
	Dihedral angle[a] (°)	ΔE [kcal mol^{-1}]	ΔG [kcal mol^{-1}]	Dihedral angle[a] (°)	ΔE [kcal mol^{-1}]	ΔG [kcal mol^{-1}]
s-*cis*/*M*	−120.6	0	0	−116.7	0	0
s-*cis*/*M*	130.8	0.85	1.08	129.0	0.66	0.28
s-*cis*/**TS_0**	5.0	9.08	11.89	0.6	9.43	9.70
s-*cis*/**TS _180**	177.3	10.07	12.47	−176.7	10.02	11.45
s-*trans*/*M*	−134.7	1.41	2.87	−130.2	0.97	1.12
s-*trans*/*P*	130.0	3.00	2.94	128.9	1.58	0.97
s-*trans*/**TS_0**	3.4	12.72	14.45	−1.1	12.78	14.04
s-*trans*/**TS _180**	179.2	10.50	11.73	179.0	10.53	11.45

[a] N6–C7–C1″–C2″ dihedral angle value.

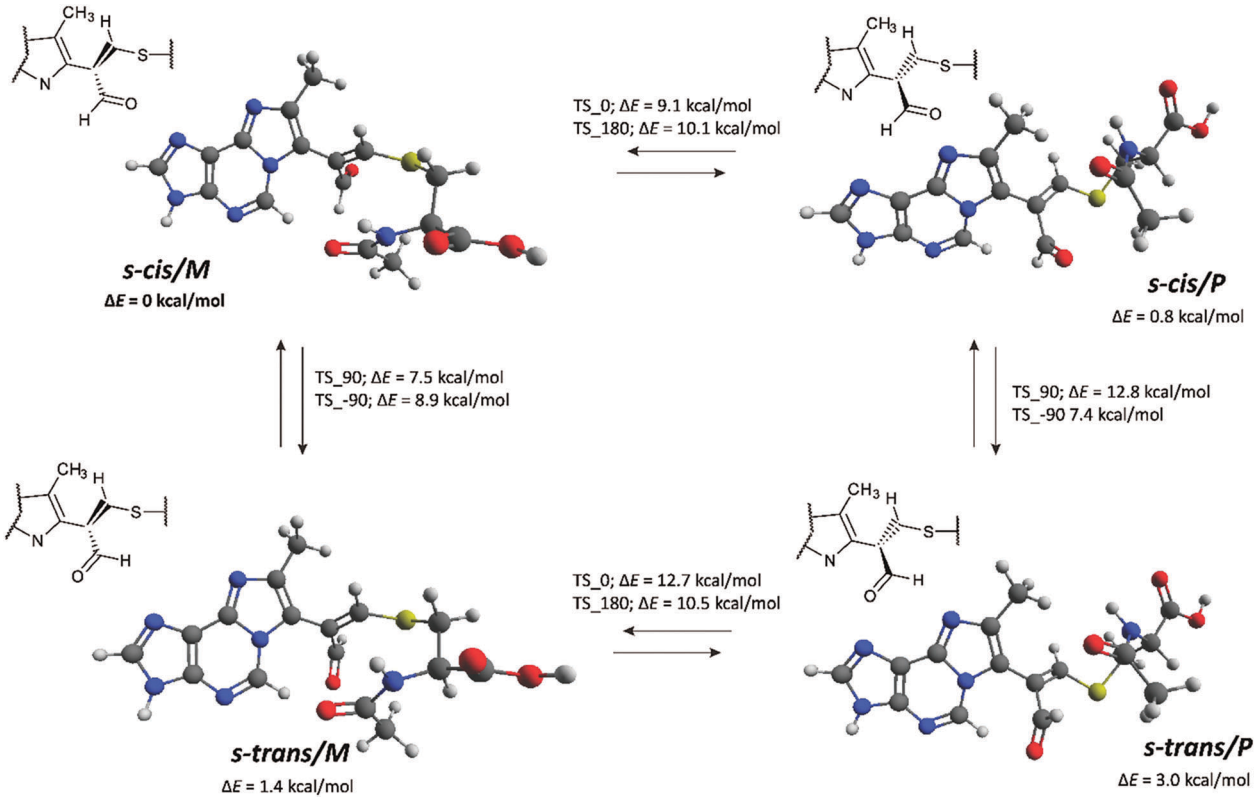

Fig. 17 Energy minima structures of **M_1MGx-Ade–NAC** and energy barriers of their interconversion (calculated at the M06/6-31G(d) level of theory *in vacuo*, see the ESI,† Fig. S42 for transition state structures).

Table 4 The relative energy values (ΔE) of s-*cis* and s-*trans* conformers of **M_1MGx-Ade–NAC** calculated using M06/6-31++G(d,p), B3LYP/6-31++G(d,p), ωB97X-D/6-31G(d) and MP2/6-31G(d) *in vacuo*. For comparison the ΔE values calculated at the initial M06/6-31G(d) level are given

	Dihedral angle[a] (°)	M06/6-31G(d)	M06/6-31++G(d,p)	B3LYP/6-31++G(d,p)	ωB97X-D/6-31G(d)	MP2/6-31G(d)
s-*cis*/*M*	−120.6	0.00	0.00	0.00	0.00	0.27
s-*cis*/*M*	130.8	0.85	1.26	0.07	1.22	1.83
s-*cis*/**TS_0**	5.0	9.08	9.29	9.24	10.68	15.22
s-*cis*/**TS _180**	177.3	10.07	10.73	10.32	11.87	17.73
s-*trans*/*M*	−134.7	1.41	1.52	1.34	1.06	0.00
s-*trans*/*P*	130.0	3.00	3.23	2.73	3.05	2.08
s-*trans*/**TS_0**	3.4	12.72	12.32	13.16	13.82	16.13
s-*trans*/**TS _180**	179.2	10.50	11.00	10.73	11.32	14.29

[a] N6–C7–C1″–C2″ dihedral angle value.

density of the total electron energy in BCPs, H_{BCP}, correlate well with the H-bond energy, so they well describe the H-bond strength, but may be applied rather for samples of related compounds.[36] For the particular case of O–H···O intermolecular hydrogen

bonds in water and methanol clusters, a reasonably good linear correlation between the charge density at the BCPs and the strength of the H-bonds was reported.[37–39] Thus, analysis of such parameters may be useful for the estimation of the relative strength of hydrogen bonding or other stabilizing interactions.[40–43]

The analysis of BCP also provides information on the nature of interatomic interaction.[44] For shared interactions like covalent and polarized bonds, the Laplacian of electron density is negative because there is concentration of electron density within the atom–atom region. For the interactions between closed-shell systems like van der Waals interactions, ionic ones, and hydrogen bonds, there is the depletion of electron charge within the atom–atom region, and hence the Laplacian is positive. Thus, the sign of the Laplacian may indicate the kind of interaction. There is a very interesting situation in the case of hydrogen bonding where usually the Laplacian is positive; however, for very strong hydrogen bonds like those in $H_5O_2^+$ or $(FHF)^-$, the Laplacians are negative, respectively, for both H···O or H···F contacts. This is the strong evidence for the covalent character of hydrogen bonding.[45]

Rozas *et al.* have classified hydrogen bonds on the basis of $\nabla^2\rho_{BCP}$ and H_{BCP} values.[46] Weak and medium strength hydrogen bonds show both positive $\nabla^2\rho_{BCP}$ and H_{BCP} values. For strong H-bonds, $\nabla^2\rho_{BCP}$ is positive and H_{BCP} is negative. For very strong hydrogen bonds, $\nabla^2\rho_{BCP}$ and consequently the H_{BCP} values are negative. Cremer and Kraka involved the energetic topological parameters into the classification of interactions much earlier.[47]

To sum up, for samples of related compounds the stronger interactions should exhibit greater value of electron density in BCPs (ρ_{BCP}), greater absolute value of the electron density's Laplacian ($\nabla^2\rho_{BCP}$) and lower value of the total electron energy in BCPs (H_{BCP}).

The above mentioned topological parameters for hydrogen bonds and other stabilizing interactions in the investigated structures are collected in Table 5. Only interactions which need to be rearranged in order to initiate the rotation $P \rightarrow M$ (or reverse) were considered as the ones which may inhibit such interconversion.

The considered topological parameters of electron density always have positive values. This indicates that there are no strong interactions which may inhibit rotation and fast interconversion between rotamers *P* and *M* at room temperature. However, the most stable conformers s-*cis*/*M* can exist as the two stable equivalent forms (having almost the same energy): one with the dihedral angle N6–C7–C1″–C2″ of about −50° (s-*cis*/M_{-50}) and the other one with the angle of about −120° (s-*cis*/M_{-120}) (both of them are having the *M* helicity). Within the form having the dihedral angle N6–C7–C1″–C2″ of about −50° in compound **M_1MGx-A-NAC** (containing a sugar moiety) there are 4 possible interactions recognized by the AIM analysis (Fig. 18).

Probably, all 4 of them simultaneously are capable of inhibiting, to some extent, rotation $M \rightarrow P$. What is interesting, is that in the analogous case of compound **M_1MGx-Ade–NAC**, the one without a sugar substituent, such rotamers have only one (C5–H···O=C_{acetyl}) of the four interactions observed in the compound containing the sugar moiety. This shows the role of sugar substitution in the stabilization of rotamer s-*cis*/*M*, where the sugar moiety is involved in interaction (C2′–OH···O=C_{acetyl}) (Fig. 18). Moreover, the one interaction in rotamer s-*cis*/M_{-50} of the compound without the sugar substituent seems to be the strongest one: having the highest value of electron density (+0.017), the highest absolute value of Laplacian (+0.053) and the lowest value of total electron energy (+0.0002).

In the case of rotamers s-*cis*/*P* there is only one interaction (C8–CH_3···O=C_{acetyl}) considered as the one which may inhibit such interconversion. Further, conformers having the aldehyde moiety in s-*trans* configuration (s-*trans*/*M* and s-*trans*/*P*) are stabilized by two interactions each (Table 5).

The difference in the topological parameter values for the corresponding interactions in compounds **M_1MGx-Ade–NAC** (without sugar) and **M_1MGx-A-NAC** (with sugar) allows us to investigate the impact of the sugar moiety on the strength of the considered interactions. All considered interactions seem to be equal or stronger for the case of compound **M_1MGx-A-NAC** containing a sugar moiety, which indicates that this compound should be less labile in the considered rotation $P \rightarrow M$ or

Table 5 Bonding characteristics: electron density, ρ_{BCP}; Laplacian of the electron densities, $\nabla^2\rho_{BCP}$; and energy density, H_{BCP}. All values in atomic units

Structure	Rotamer	Complex	ρ_{BCP}	$\nabla^2\rho_{BCP}$	H_{BCP}
M_1MGx-Ade–NAC	s-*cis*/M_{-50}	C5–H···O=C_{acetyl}	+0.017	+0.053	+0.0002
	s-*cis*/M_{-120}	C5—H···O=C_{acetyl}	+0.008	+0.032	+0.0013
	s-*cis*/*P*	C8–CH_3···O=C_{acetyl}	+0.014	+0.044	+0.0003
	s-*trans*/*M*	C5–H···O=$C_{aldehyde}$	+0.010	+0.041	+0.0017
		C5–H···O=C_{acetyl}	+0.013	+0.047	+0.0010
	s-*trans*/*P*	C5–H···O=$C_{aldehyde}$	+0.012	+0.048	+0.0015
		C8–CH_3···O=C_{acetyl}	+0.014	+0.042	+0.0002
M_1MGx-A-NAC	s-*cis*/M_{-50}	C5–H···O=C_{acetyl}	+0.013	+0.047	+0.0011
		C5–H···C2″	+0.009	+0.034	+0.0018
		N4···O=C_{acetyl}	+0.008	+0.028	+0.0006
		C2′–OH···O=C_{acetyl}	+0.008	+0.034	+0.0011
	s-*cis*/M_{-120}	C5–H···O=C_{acetyl}	+0.011	+0.042	+0.0012
	s-*cis*/*P*	C8–CH_3···O=C_{acetyl}	+0.014	+0.045	+0.0003
	s-*trans*/*M*	C5···O=$C_{aldehyde}$	+0.010	+0.042	+0.0017
		C5–H···O=C_{acetyl}	+0.014	+0.050	+0.0009
	s-*trans*/*P*	C5–H···O=$C_{aldehyde}$	+0.013	+0.052	+0.0015
		C8–CH_3···O=C_{acetyl}	+0.014	+0.042	+0.0001

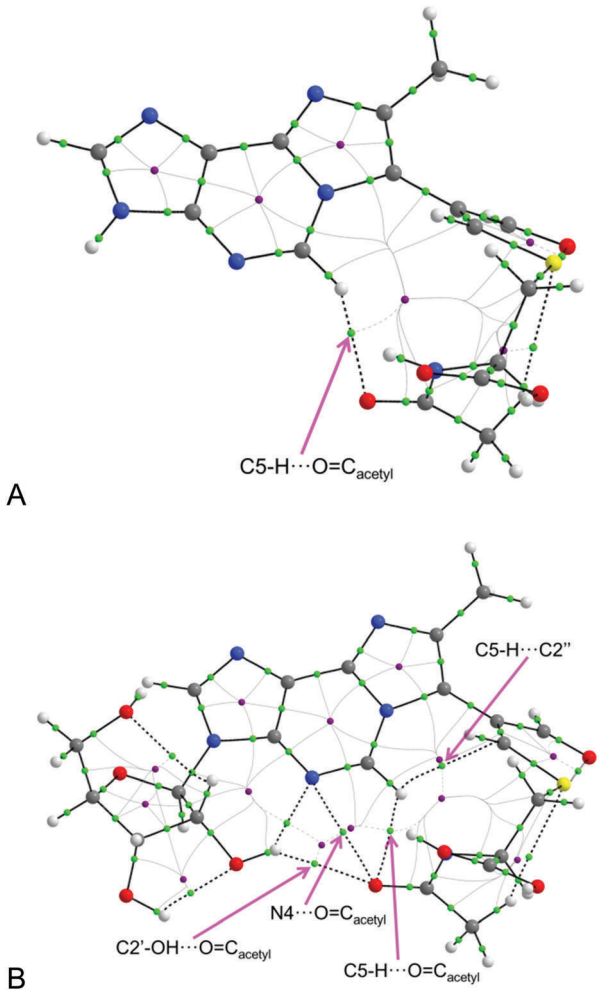

Fig. 18 The bond paths (black lines), bond critical points (small green dots), ring critical points (small purple dots) and interatomic surfaces (grey lines) for rotamer s-*cis*/M_{-50} of compound **M_1MGx-Ade–NAC** (A) and **M_1MGx-A-NAC** (B).

reverse (assuming the same energy barrier). However, relatively low differences in the discussed numerical values do not allow us to make clear statements.

Conclusions

We studied the reactivity of the aldehydic adenine nucleoside adducts towards *N*-acetylcysteine and provided structural characterization of cross-links that could be induced by DNA adducts containing carbonyl moieties, in reactions with the cysteine residues of proteins.

Bifunctional carbonyl compounds of endogenous origin are considered to be responsible for different types of cross-link formation.[48] Such carbonyls are known to form adducts with nucleophilic biomolecules and these adducts can further undergo interactions with other cellular macromolecules giving rise to cross-linked products.[49,50] Our investigations show that such mechanisms can be, at least in part, valid also for cysteine containing cross-link formation. It is well known that cysteine residues are involved in the catalytic activity of enzymes. Moreover the cysteine thiol groups take part in disulfide bond formation which plays an important role in protein structure stabilization. Therefore structural modifications of such sites can have broad functional implications. As strong nucleophilic centers, the cysteine thiol groups are very probable targets for electrophilic attack that leads to DPC formation. Despite their ubiquitous presence in living cells, the structural features of DPCs and the mechanisms of their formation still remain to be explored. The literature reports on cysteine containing DPC synthesis and structural determination do not refer to the stability of such lesions. Our results show that stability studies seem to be crucial for establishing the biological importance of cysteine containing DPCs and for clarifying the role that the amino acid plays in their formation. Our results also provide insight into the chemical nature of the cross-links possibly induced by α,β-unsaturated carbonyl compounds between the adenine residues of DNA and cysteine residues of proteins. The highest yield of *N*-acetylcysteine cross-link formation was observed in reactions performed at a pH of about 3. This fact does not exclude the possibility of such cross-link formation *in vivo* because they were also found to be formed (in smaller amounts) under physiological conditions. Apart from that different cellular compartments are characterized by individual environments including pH. It is worth noticing that our studies provide the first discussion on the acidity/neutrality of the cysteine containing reaction medium, and pH was shown to be a key factor for the formation of *N*-acetylcysteine cross-links.

The mechanism proposed for *N*-acetylcysteine cross-link degradation and transformation gives a clear explanation for difficulties in detecting and isolating such lesions. Fast transformation of the cysteine cross-links occurring in the presence of the lysine was probably the reason for a much lower yield of the methylglyoxal induced cross-links between cysteine residues of DNA Klenow fragment polymerase and guanine residues of the substrate DNA compared to analogous cross-links involving the lysine residues.[25] Difficulties in detecting cysteine containing cross-links do not rule out the high probability of such lesion formation *in vivo*.

Experimental

Materials

1,1,3,3-Tetramethoxypropane (TMP), 2′-deoxyadenosine monohydrate, adenosine, adenine, methylglyoxal solution (40 wt% in H_2O), glyoxal solution (40 wt% in H_2O), *N*-acetylcysteine, N^{α}-acetyllysine, NH_4HCO_3, ACN (gradient grade for chromatography), and D_2O (containing 0.05% TSP-d_4) were purchased from Sigma-Aldrich.

Chromatographic methods

Progress of the reactions was monitored by LC-DAD and the analyses were performed on an Agilent 1100 series liquid chromatographic system consisting of a binary pump (G1312A), autosampler (G1313A), vacuum degasser (G1379A), diode-array detector (UV; G1315B), 5 μm, 4.6 × 150 mm reversed-phase C18 anal. column

(Hypersil BDS, Thermo Scientific) and Agilent ChemStation data handling program (Agilent Technologies). The column was eluted isocratically for 5 min with 0.01 M phosphate buffer, pH 7.1, and then with a gradient from 0% to 20% ACN in 20 min at a flow rate of 1.5 mL min^{-1}.

Separation and purification of the synthesized compounds was carried out using an Agilent 1200 Series HPLC system consisting of a binary pump (G1312A), vacuum degasser (G1379B), autosampler (G1329A), thermostated column compartment (G1316A), diode-array detector (UV; G1315B), fraction collector (G1364C), and Agilent ChemStation data handling program (Agilent Technologies). 1.2 mM NH_4HCO_3 and ACN were used as eluents. The flow was set to 3 mL min^{-1}. Isolation of **M_1Gx-A**, **M_1MGx-A** and **M_1MGx-dA** was performed using a semiprep. 5 μm, 10 × 250 mm (Hypersil BDS, Thermo Scientific) reversed-phase C18 column thermostated at 25 °C. Isolation of **M_1Gx-A-NAC**, **M_1MGx-A-NAC**, **M_1MGx-dA** and **M_1MGx-Ade–NAC** was carried out by the use of a semiprep. 5 μm, 10 × 250 mm (Hypersil GOLD, Thermo Scientific) reversed-phase C18 column thermostated at 20 °C.

ESI-LC/MS and ESI-LC/MS/MS analyses

ESI-LC/MS and ESI-LC/MS/MS analyses were performed with an Agilent 1200 LC system using an Agilent Q-TOF 6540 spectrometer with a DUAL AJS ESI source. Ionization was carried out using nitrogen as the nebulizing/drying gas (8 L min^{-1}, 300 °C, 35 psi) and sheath gas (11 L min^{-1}, 325 °C). The VCap was set to 3500 V, the fragmentor was set to 100 V. Ion polarity mode and collision energy values for MS/MS experiments were chosen individually and given with the appropriate spectra. The analyzed compounds were introduced through the LC system using a reversed phase analytical column (5 μm, 4.6 mm × 150 mm, Thermo Scientific) and eluted isocratically for 3 min with water, and then with a gradient from 0% to 20% of ACN for 20 min with a flow rate of 0.5 min min^{-1}. The thermostat was set to 25 °C.

General procedure for M_1Gx-A, M_1MGx-dA and M_1MGx-A synthesis

M_1Gx-A, **M_1MGx-dA**, and **M_1MGx-A** were synthesized by using a modified procedure developed earlier in our laboratory.[28] Malonaldehyde was prepared *in situ* by the acidic hydrolysis of 1,1,3,3-tetramethoxypropane (TMP).[51] Syntheses of the adducts were accomplished according to the methods published previously.[29]

Studies on M_1Gx-A, M_1MGx-dA and M_1MGx-A reactivity towards *N*-acetylcysteine (analytical-scale reactions)

Reaction of M_1Gx-A with *N*-acetylcysteine. *N*-acetylcysteine (3.6 mg, 22.6 μmol) was dissolved in a solution of **M_1Gx-A** (0.8 mg, 2.26 μmol) in 0.5 mL of 0.1 M phosphate buffer (pH 7.4). The mixture was divided into two parts and incubated at 37 °C and 50 °C, respectively. Progress of the reactions was monitored by LC-DAD.

Reaction of M_1MGx-A with *N*-acetylcysteine. *N*-Acetylcysteine (35 mg, 0.21 mmol) was dissolved in a solution of **M_1MGx-A** (8 mg, 0.021 mmol) in 0.8 mL of 0.1 M phosphate buffer (pH 7.4). The mixture was divided into two parts and incubated at 37 °C and 50 °C, respectively. Progress of the reactions was monitored by LC-DAD.

Reaction of M_1MGx-dA with *N*-acetylcysteine. *N*-Acetylcysteine (4.5 mg, 27.6 μmol) was dissolved in a solution of **M_1MGx-dA** (1 mg, 2.79 μmol) in 0.4 mL of 0.1 M phosphate buffer (pH 7.4) and of 1 M phosphate buffer (pH 7.4), respectively. Both mixtures were divided into two parts and incubated at 37 °C and 50 °C, respectively. Progress of the reactions was monitored by LC-DAD.

M_1MGx-dA–NAC HRMS calc. for $C_{21}H_{25}N_6O_7S^+$ $[M + H]^+$ m/z = 505.1500, found m/z = 505.1494 (error 1.2 ppm).

M_1MGx-Ade–NAC HRMS calc. for $C_{16}H_{17}N_6O_4S^+$ $[M + H]^+$ m/z = 389.1027, found m/z = 389.1021 (error 1.5 ppm).

Reaction of M_1Gx-A with *N*-acetylcysteine and N^{α}-acetyllysine. *N*-Acetylcysteine (2.7 mg, 27.7 μmol) and N^{α}-acetyllysine (3.1 mg, 27.7 μmol) were added to the solution of **M_1Gx-A** (1 mg, 2.77 μmol) in 0.5 mL of 0.1 M phosphate buffer (pH 7.4). The pH was adjusted to 3 using acetic acid. The mixture was kept at 37 °C for 7 days and analyzed using LC-DAD and LC-MS systems.

Synthesis of cross-links

Synthesis of M_1Gx-A-NAC. *N*-Acetylcysteine (59 mg, 0.36 mmol) was dissolved in a solution of **M_1Gx-A** (13 mg, 0.036 mmol) in 1.3 mL of 0.1 M phosphate buffer (pH 7.4). The reaction was carried out at 50 °C for 24 h. For isolation of **M_1Gx-A-NAC** the semiprep. HPLC column was eluted with a gradient from 1% to 10% of ACN for 26 min. The fractions containing the pure product were combined, evaporated to dryness and lyophilized. The resulting **M_1Gx-A-NAC** (4.5 mg, yield: 25%) was subjected to spectroscopic and spectrometric studies.

M_1Gx-A-NAC HRMS calc. for $C_{20}H_{23}N_6O_8S^+$ $[M + H]^+$ m/z = 507.1293, found m/z = 507.1283 (error 2.0 ppm).

Synthesis of M_1MGx-A-NAC. *N*-Acetylcysteine (250.8 mg, 1.5 mmol) was dissolved in a solution of **M_1MGx-A** (57.7 mg, 0.15 mmol) in 5.7 mL of 0.1 M phosphate buffer (pH 7.4). The reaction was carried out at 50 °C for 24 h. For isolation of the major product the semiprep. HPLC column was eluted with a gradient from 1% to 10% of ACN for 20 min. The fractions containing the pure product were combined, evaporated to dryness and lyophilized. The resulting **M_1MGx-A-NAC** (22 mg, yield: 28%) was subjected to spectroscopic and spectrometric studies.

M_1MGx-A-NAC HRMS calc. for $C_{21}H_{25}N_6O_8S^+$ $[M + H]^+$ m/z = 521.1449, found m/z = 521.1448 (error 0.2 ppm).

Synthesis of M_1MGx-Ade–NAC. *N*-Acetylcysteine (122.1 mg, 7.5 mmol) was dissolved in a solution of **M_1MGx-Ade** (18.2 mg, 0.75 mmol) in 2 mL of 0.1 M phosphate buffer (pH 7.4). The reaction was carried out at 50 °C for 24 h. For isolation of the major product the semiprep. HPLC column was eluted with a gradient from 1% to 10% of ACN for 20 min. The fractions containing the pure product were combined, evaporated to dryness and lyophilized. The resulting **M_1MGx-Ade–NAC** (9 mg, yield: 31%) was subjected to spectroscopic and spectrometric studies.

Stability studies of M_1Gx-A, M_1MGx-Ade–NAC and M_1MGx-A-NAC. **M_1MGx-Ade–NAC** (1 mg, 2.6 μmol) and **M_1MGx-A-NAC** (1 mg, 1.9 μmol) were dissolved separately in 0.2 mL of both 0.1 M and 1 M phosphate buffer. **M_1Gx-A-NAC** (1 mg, 2 μmol) was dissolved in 0.2 mL of 0.1 M phosphate buffer. The mixtures were kept at 37 °C for 30 days. N^{α}-Acetyllysine was dissolved in the solutions of **M_1MGx-A-NAC** and **M_1Gx-A-NAC** in 0.1 M

phosphate buffer and incubated at 37 °C for 7 days. Aliquots of the reaction mixtures were analyzed by using LC-DAD and LC-MS.

M_1Gx-A HRMS calc. for $C_{15}H_{16}N_5O_6^+$ $[M + H]^+$ m/z = 362.1095, found m/z = 362.1101 (error 1.7 ppm).

M_1Gx-A-NH2 HRMS calc. for $C_{15}H_{17}N_6O_5^+$ $[M + H]^+$ m/z = 361.1255, found m/z = 361.1257 (error 0.6 ppm).

M_1MGx-Ade HRMS calc. for $C_{11}H_{10}N_5O_2^+$ $[M + H]^+$ m/z = 244.0829, found m/z = 244.0824 (error 2.0 ppm).

M_1MGx-Ade-NH_2 HRMS calc. for $C_{11}H_{11}N_6O^+$ $[M + H]^+$ m/z = 243.09889, found m/z = 243.0989 (error 0.04 ppm).

M_1MGx-A HRMS calc. for $C_{16}H_{18}N_5O_6^+$ $[M + H]^+$ m/z = 376.1252, found m/z = 376.1247 (error 1.3 ppm).

M_1MGx-A-NH2 HRMS calc. for $C_{16}H_{19}N_6O_5^+$ $[M + H]^+$ m/z = 375.1411, found m/z = 375.1408 (error 0.8 ppm).

M_1Gx-A-N^{α}AcLys HRMS calc. for $C_{23}H_{30}N_7O_8^+$ $[M + H]^+$ m/z = 532.2150, found m/z = 532.2139 (error 2.1 ppm).

M_1Gx-A-(N^{α}AcLys)2 HRMS calc. for $C_{31}H_{44}N_9O_{10}^+$ $[M + H]^+$ m/z = 702.3206, found m/z = 702.3199 (error 1.0 ppm).

M_1MGx-A-N^{α}AcLys HRMS calc. for $C_{24}H_{32}N_7O_8^+$ $[M + H]^+$ m/z = 546.2307. found m/z = 546.2299 (error 1.5 ppm).

M_1MGx-A-(N^{α}AcLys)$_2$ HRMS calc. for $C_{32}H_{46}N_9O_{10}^+$ $[M + H]^+$ m/z = 716.3362, found m/z = 716.3354 (error 1.1 ppm).

NMR spectroscopy

Samples were dissolved in D_2O (internal standard: 3-(trimethylsilyl)propionic-2,2,3,3-d_4 acid sodium salt, TSP-d_4). The experiments were performed at the temperature of 298 K. All spectra were acquired on a Bruker Avance III DRX system, operating at frequencies of 600.3 MHz (^{1}H) and 150.9 MHz (^{13}C). The spectrometer was equipped with a 5 mm triple-resonance inverse probe head [^{1}H/^{31}P/BB]. High-power ^{1}H and ^{13}C $\pi/2$ pulses of 9.00 and 15.00 μs, respectively, were used. 1D and 2D homo- and heteronuclear correlation experiments were carried out by using pulse sequences from the Bruker pulse program library.

For the variable-temperature ^{1}H NMR experiments samples of **M_1MGx-Ade–NAC** and **M_1MGx-A-NAC** in D_2O were thermostated for 1 h before measurement. 100% ethylene glycol recommended for studies at higher temperatures[52] was used for creating a temperature calibrating curve (ESI,† Table S2 and Charts S1, S2).

Calculation methods

The initial structures of **M_1MGx-A-NAC** and **M_1MGx-Ade–NAC** were generated based on average bond lengths and valence angles; dihedral angles for rotatable bonds were sampled randomly. All initial conformers of **M_1MGx-A-NAC** (12) and **M_1MGx-Ade–NAC** (12) were optimized at the M06/6-31G(d) level of theory as isolated molecules. The lowest energy conformers of the s-*cis* and the s-*trans* series of both structures were selected for further research. These structures were optimized at the M06/6-31G(d) level in the gas phase with a frozen N6–C7–C1″–C2″ dihedral angle in steps of 10°, so full rotation around the C7–C1″ bond was performed. The lowest energy values found for the conformers of **M_1MGx-A-NAC** and **M_1MGx-Ade–NAC** were taken as a relative energy of 0 kcal mol^{-1}. Transition states **TS_0** and **TS_180** of the s-*cis* and s-*trans* conformers were found and optimized at the same level of theory. The Gibbs free energies were calculated on the basis of energy thermal correction for minima and transition states. To take into account the effect of solvent (water) the minima and transition state structures were reoptimized at the M06/6-31G(d) level using the polarizable continuum model (PCM). Both the relative energies and Gibbs free energies were calculated. The relative energies in single points for isolated molecules were also calculated by using the following methods: M06/6-31++G(d,p), B3LYP/6-31++G(d,p) and MP2/6-31G(d). Geometry optimization and energy calculations were performed by using Gaussian 09.[53]

The energy barriers between rotamers of **M_1MGx-A-NAC** and **M_1MGx-Ade–NAC** calculated by the use of quantum-chemical methods were compared with those obtained on the basis of variable-temperature ^{1}H NMR experiments.

Atoms in molecules theory was used for the investigation of intramolecular interactions in the structures of **M_1MGx-A-NAC** and **M_1MGx-Ade–NAC** in their minima. Parameters: electron density in bond critical points (BCPs), ρ_{BCP}, its Laplacian, $\nabla^2\rho_{BCP}$ and density of the total electron energy in BCP, H_{BCP}, were computed using the AIMAll program.[54]

Acknowledgements

This research was supported in part by PL-Grid Infrastructure (http://www.plgrid.pl/en), and the authors are thankful for help with the figures. The authors thank Perlan Technologies Polska Sp. z o. o. for providing the HPLC/Q-TOF Agilent 1260/6540 instrument.

References

1 S. Barker, M. Weinfeld and D. Murray, *Mutat. Res.*, 2005, **589**, 111–135.
2 N. Y. Tretyakova, A. Groehler and S. Ji, *Acc. Chem. Res.*, 2015, **48**, 1631–1644.
3 H. Ide, M. I. Shoulkamy, T. Nakano, M. Miyamoto-Matsubara and A. M. H. Salem, *Mutat. Res., Fundam. Mol. Mech. Mutagen.*, 2011, **711**, 113–122.
4 E. J. Wurtmann and S. L. Wolin, *Crit. Rev. Biochem. Mol. Biol.*, 2009, **44**, 34–49.
5 K. Möller, J. Rinke, A. Ross, G. Buddle and R. Brimacombe, *Eur. J. Biochem.*, 1977, **76**, 175–187.
6 P. Casati, *Plant Physiol.*, 2004, **136**, 3319–3332.
7 S. Wickramaratne, E. J. Boldry, C. Buehler, Y. C. Wang, M. D. Distefano and N. Y. Tretyakova, *J. Biol. Chem.*, 2015, **290**, 775–787.
8 S. Wickramaratne, S. Ji, S. Mukherjee, Y. Su, M. G. Pence, L. Lior-Hoffmann, I. Fu, S. Broyde, F. P. Guengerich, M. Distefano, O. D. Schärer, Y. Y. Sham and N. Tretyakova, *J. Biol. Chem.*, 2016, **291**, 23589–23603.
9 C.-Y. Tu, Y.-F. Chen, C.-K. Lii and T.-S. Wang, *Toxicol. In Vitro*, 2013, **27**, 1211–1219.
10 H.-J. C. Chen, W.-L. Chiu, W.-P. Lin and S.-S. Yang, *ChemBioChem*, 2008, **9**, 1074–1081.

11 N. Murata-Kamiya and H. Kamiya, *Nucleic Acids Res.*, 2001, **29**, 3433–3438.
12 S. Barker, M. Weinfeld, J. Zheng, L. Li and D. Murray, *J. Biol. Chem.*, 2005, **280**, 33826–33838.
13 T. B. Gherezghiher, X. Ming, P. W. Villalta, C. Campbell and N. Y. Tretyakova, *J. Proteome Res.*, 2013, **12**, 2151–2164.
14 H. Qiu and Y. Wang, *J. Proteome Res.*, 2009, **8**, 1983–1991.
15 R. L. Loeber, E. D. Michaelson-Richie, S. G. Codreanu, D. C. Liebler, C. R. Campbell and N. Tretyakova, *Chem. Res. Toxicol.*, 2009, **22**, 1151–1162.
16 T. B. Gherezghiher, X. Ming, P. W. Villalta, C. Campbell and N. Y. Tretyakova, *J. Proteome Res.*, 2013, **12**, 2151–2164.
17 A. Groehler, P. W. Villalta, C. Campbell and N. Tretyakova, *Chem. Res. Toxicol.*, 2016, **29**, 190–202.
18 J. M. Aćimović, B. D. Stanimirović, N. Todorović, V. B. Jovanović and L. M. Mandić, *Chem.-Biol. Interact.*, 2010, **188**, 21–30.
19 H. Kasai, N. Iwamoto-Tanaka and S. Fukada, *Carcinogenesis*, 1998, **19**, 1459–1465.
20 R. Loeber, E. Michaelson, Q. Fang, C. Campbell, A. E. Pegg and N. Tretyakova, *Chem. Res. Toxicol.*, 2008, **21**, 787–795.
21 R. Loeber, M. Rajesh, Q. Fang, A. E. Pegg and N. Tretyakova, *Chem. Res. Toxicol.*, 2006, **19**, 645–654.
22 E. D. Michaelson-Richie, R. L. Loeber, S. G. Codreanu, X. Ming, D. C. Liebler, C. Campbell and N. Y. Tretyakova, *J. Proteome Res.*, 2010, **9**, 4353–4367.
23 D. L. Carbone, J. A. Doorn, Z. Kiebler and D. R. Petersen, *Chem. Res. Toxicol.*, 2005, **18**, 1324–1331.
24 D. R. Seiner, J. N. LaButti and K. S. Gates, *Chem. Res. Toxicol.*, 2007, **20**, 1315–1320.
25 K. V. Petrova, A. D. Millsap, D. F. Stec and C. J. Rizzo, *Chem. Res. Toxicol.*, 2014, **27**, 1019–1029.
26 S. Barker, D. Murray, J. Zheng, L. Li and M. Weinfeld, *Anal. Biochem.*, 2005, **344**, 204–215.
27 L. L. G. Carrette, T. Morii and A. Madder, *Bioconjugate Chem.*, 2013, **24**, 2008–2014.
28 D. Pluskota-Karwatka, A. J. Pawłowicz, M. Bruszyńska, A. Greszkiewicz, R. Latajka and L. Kronberg, *Chem. Biodiversity*, 2010, **7**, 959–974.
29 K. Salus, M. Hoffmann, B. Wyrzykiewicz and D. Pluskota-Karwatka, *New J. Chem.*, 2016, **40**, 3875–3884.
30 D. Pluskota-Karwatka, D. Matysiak, M. Makarewicz and L. Kronberg, *Eur. J. Org. Chem.*, 2012, 4797–4804.
31 R. Drożdż, J. W. Naskalski and J. Sznajd, *Biochim. Biophys. Acta, Protein Struct. Mol. Enzymol.*, 1988, **957**, 47–52.
32 E. R. Stadtman and B. S. Berlett, *J. Biol. Chem.*, 1991, **266**, 17201–17211.
33 J. Cai, A. Bhatnagar and W. M. Pierce, *Chem. Res. Toxicol.*, 2009, **22**, 708–716.
34 H. Shanan-Atidi and K. H. Bar-Eli, *J. Phys. Chem.*, 1970, **74**, 961–963.
35 R. F. W. Bader, *Atoms in Molecules: A Quantum Theory*, Oxford University Press, Oxford England: New York, 1st Paperback edn, 1994.
36 S. J. Grabowski, *J. Phys. Chem. A*, 2001, **105**, 10739–10746.
37 O. Mó, M. Yáñez and J. Elguero, *J. Chem. Phys.*, 1992, **97**, 6628–6638.
38 O. Mó, M. Yáñez and J. Elguero, *THEOCHEM*, 1994, **314**, 73–81.
39 L. González, O. Mó and M. Yáñez, *J. Phys. Chem. A*, 1997, **101**, 9710–9719.
40 E. Espinosa, M. Souhassou, H. Lachekar and C. Lecomte, *Acta Crystallogr., Sect. B: Struct. Sci.*, 1999, **55**, 563–572.
41 C. Gatti, V. R. Saunders and C. Roetti, *J. Chem. Phys.*, 1994, **101**, 10686–10696.
42 S. J. Grabowski, *J. Mol. Struct.*, 2001, **562**, 137–143.
43 J. Murgich, H. J. Franco and G. San-Blas, *J. Phys. Chem. A*, 2006, **110**, 10106–10115.
44 R. F. W. Bader and H. Essén, *J. Chem. Phys.*, 1984, **80**, 1943–1960.
45 S. J. Grabowski, *Chem. Rev.*, 2011, **111**, 2597–2625.
46 I. Rozas, I. Alkorta and J. Elguero, *J. Am. Chem. Soc.*, 2000, **122**, 11154–11161.
47 D. Cremer and E. Kraka, *Croat. Chem. Acta*, 1984, **57**, 1259–1281.
48 M. P. Stone, Y.-J. Cho, H. Huang, H.-Y. Kim, I. D. Kozekov, A. Kozekova, H. Wang, I. G. Minko, R. S. Lloyd, T. M. Harris and C. J. Rizzo, *Acc. Chem. Res.*, 2008, **41**, 793–804.
49 I. D. Kozekov, R. J. Turesky, G. R. Alas, C. M. Harris, T. M. Harris and C. J. Rizzo, *Chem. Res. Toxicol.*, 2010, **23**, 1701–1713.
50 M. Sanchez, I. D. Kozekov, T. M. Harris and R. S. Lloyd, *Chem. Res. Toxicol.*, 2005, **18**, 1683–1690.
51 K. Stone, A. Uzieblo and L. J. Marnett, *Chem. Res. Toxicol.*, 1990, **3**, 467–472.
52 C. Ammann, P. Meier and A. E. Merbach, *J. Magn. Reson.*, 1982, **46**, 319–321.
53 Gaussian 09 Citation http://www.gaussian.com/g_tech/g_ur/m_citation.htm, accessed Sep 11, 2015.
54 AIMAll (Version 16.01.09), Todd A. Keith, TK Gristmill Software, Overland Park KS, USA, 2016 (aim.tkgristmill.com) http://aim.tkgristmill.com/, accessed May 2, 2016.